



HAL
open science

Effective properties of linear random materials: application to Al/SiC and resin/glass composites

Serge Dumont, Frédéric Lebon

► **To cite this version:**

Serge Dumont, Frédéric Lebon. Effective properties of linear random materials: application to Al/SiC and resin/glass composites. *Computational Mechanics*, 2008, 42, pp.775-786. 10.1007/s00466-008-0280-4 . hal-00346031

HAL Id: hal-00346031

<https://hal.science/hal-00346031>

Submitted on 1 Jun 2018

HAL is a multi-disciplinary open access archive for the deposit and dissemination of scientific research documents, whether they are published or not. The documents may come from teaching and research institutions in France or abroad, or from public or private research centers.

L'archive ouverte pluridisciplinaire **HAL**, est destinée au dépôt et à la diffusion de documents scientifiques de niveau recherche, publiés ou non, émanant des établissements d'enseignement et de recherche français ou étrangers, des laboratoires publics ou privés.

Effective properties of linear random materials: application to Al/SiC and resin/glass composites

Serge Dumont · Frédéric Lebon

Abstract Here we present a statistical study on the effective linear properties of random materials, i.e., microstructures which are random lattices described by a stochastic process. The local numerical procedure associated with the homogenization methods used here was based on a wavelet-element method. The resulting numerical results are compared with those obtained using classical theories. A new approach was developed in order to determine the effective properties in cases where the characteristics of the microstructure are not known.

Keywords Random materials · Wavelet-element method · Homogenization · Elasticity

1 Introduction

The aim of this study was to determine and compute the effective properties of linear random heterogeneous media. Although natural geomaterials are heterogeneous, they are generally regarded as homogeneous materials with effective properties which determine the overall behavior. Grounds, for example, are usually modeled as a body consisting of homogeneous materials with these effective properties. The behavior of these grounds cannot be predicted if the effective properties are not exactly determined. The need to

incorporate more detailed information about the microstructure is now widely recognized. During the last few years, many studies have been published presenting measurements and describing empirical and theoretical techniques for determining these effective properties. The numerical cost of solving this problem directly for each material sample would obviously be prohibitive. We previously presented a method involving a numerical scheme combined with homogenization techniques which can be used to account for the details of microstructures [9–12,24]. These algorithms based on wavelet analysis make it possible to predict the effective properties from microstructural data and thus to optimally design linear composite materials from real images of the sample.

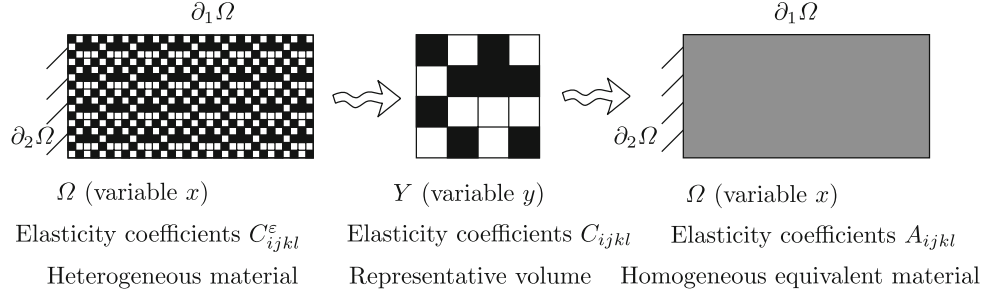
Unfortunately, in most cases, the microstructural details are not exactly known, and the effective properties are therefore assessed from statistical studies. In a well-known paper [34], Torquato (see also [35]) presented results obtained on a case where some statistical informations, such as the correlation functions, was available. This improves the bounds of the effective properties of two-phase random heterogeneous media. Results of other kinds have been published in [23,30]. Here it is assumed that only the volume fraction of each phase is known, and it is proposed to find the average effective properties of the composite. In addition, the microstructure is assumed to be given pixel by pixel, i.e., the characteristic shape of the microstructural components is taken to be a small square and its characteristic length to be the length of the pixel.

We will not discuss here the size of the representative volume, which is often a real problem with materials of this kind. We will assume the Hill's condition to be valid (see [18,37,38]) and that exists a representative volume on which we will work. For further details on the problem of choosing a sample when there exists no representative volume, we refer

S. Dumont
Laboratoire Amiénois de Mathématiques Fondamentales et Appliquées, Université de Picardie Jules Verne,
CNRS UMR 6140, 33 rue Saint Leu, 80039 Amiens, France
e-mail: serge.dumont@u-picardie.fr

F. Lebon
Laboratoire de Mécanique et d'Acoustique,
Université de Provence Aix-Marseille 1, CNRS UPR 7051, 31
chemin Joseph Aiguier, 13402 Marseille Cedex 20, France

Fig. 1 The homogenization process



to [17, 20–22]. In addition, the method proposed in previous papers is improved here. In [9] only Daubechies wavelets are used. In this paper B-spline wavelets are introduced. It will be shown below how these functions improve the numerical procedure.

In Sect. 2, the notations used are presented and the mechanical problem is defined. Section 3 is devoted to the numerical algorithm. In Sect. 4, a statistical study on AISiC and resin–glass composites is presented. The results obtained are compared with the Hashin and Shtrikman bounds [16] and with the self-consistent schema [19, 28]. At the end of the paper, the future perspectives of this approach are discussed.

2 The mechanical problem

Here it is proposed to study the behavior of a heterogeneous medium consisting of a two-phase isotropic elastic composite. A homogenization step is first performed, consisting in determining the effective properties of the equivalent homogeneous medium. Let us take a plane periodic composite Ω (macro-scale, variable x) and a rectangular periodicity cell Y (micro-scale, variable y). The bonds at all the interfaces of the composite are assumed to be perfect.

The elasticity coefficients C_{ijkl}^ε are assumed to be periodic, with period Y . We take the boundary $\partial\Omega$ of Ω to be split into two parts: $\partial\Omega = \partial_1\Omega \cup \partial_2\Omega$ with $\partial_1\Omega \cap \partial_2\Omega = \emptyset$. A traction force equal to F is imposed on $\partial_1\Omega$, and the displacement vanishes at $\partial_2\Omega$ (see Fig. 1).

In the elastostatic framework, the problem (P_ε) can be written

$$\begin{aligned} & \text{Problem}(P_\varepsilon) \\ & \text{Find } u^\varepsilon \in V \text{ such that } a_\varepsilon(u^\varepsilon, v) = L(v), \\ & \forall v \in V, \end{aligned}$$

$$\text{where } a_\varepsilon(u, v) = \int_{\Omega} C_{ijkl}^\varepsilon e_{kl}(u) e_{ij}(v) dx,$$

$$e_{kl}(u) = \frac{1}{2}(u_{k,l} + u_{l,k}),$$

$$L(v) = \int_{\Omega} f v dx + \int_{\partial_1 \Omega} F v dl,$$

$$\text{and } V = \{v \in (H^1(\Omega))^2, v = 0 \text{ on } \partial_2\Omega\}.$$

When $\varepsilon \rightarrow 0$, it has been established (see for example [3, 31]) that the solution of the previous problem u^ε tends to u in V , the space of the admissible global displacements, where u is the solution of problem P

$$\begin{aligned} & \text{Problem}(P) \\ & \text{Find } u \in V \text{ such that } a(u, v) = L(v), \forall v \in V, \end{aligned}$$

$$\text{where } a(u, v) = \int_{\Omega} A_{ijkl} e_{kl}(u) e_{ij}(v) dx$$

$$\text{and } A_{ijkl} = \frac{1}{\text{meas}(Y)} \int_Y (C_{ijkl} + C_{ijpq} e_{pq}(u^{kl})) dy.$$

To determine the displacements u^{kl} , it is necessary to solve three local problems on Y (Problem P_Y) in the space $H = (H_{\text{per}}^1(Y))^2$, the set of admissible local displacements:

$$\begin{aligned} & \text{Problem}(P_Y) \\ & E^{kl} \text{ being given, find } u^{kl} \in H \text{ such that} \end{aligned}$$

$$a_Y(u^{kl}, v) = l(v), \quad \forall v \in H, \quad (1)$$

$$\begin{aligned} \text{where } a_Y(u, v) &= \int_Y C_{klst}(y) e_{kl}(u) e_{st}(v) dy \text{ and } l(v) = \\ & - \int_Y C_{klst}(y) E^{kl} e_{st}(v) dy. \end{aligned}$$

Comment 1 Even if each component of the composite is isotropic so that the elasticity coefficients can be written using only the bulk and shear moduli K and μ , the homogeneous equivalent material is not necessarily isotropic and the elasticity tensor cannot be written using bulk and shear moduli.

3 Numerical procedure

In order to avoid having to remesh the cell Y after each draw, we decided to discretize problem P_Y with a meshless method, the wavelet element method [7, 9]. Moreover, as we will see below, the elements of the stiffness matrix can be computed with this method once and for all, without having to use quadrature formulae. Thanks to the localization

of the wavelets in both the physical and spectral spaces, the stiffness matrix is not ill conditioned. This gives a good rate of convergence for solving the linear systems [10].

This method can also be said to be a compromise between finite elements [15] and Fourier analysis [27] methods.

Periodic conditions were applied here to the boundary of the cell Y , but boundary conditions of other kinds can be used with wavelet transforms, such as vanishing displacements [14].

3.1 Daubechies wavelets

In this section, we will briefly describe Daubechies wavelets [7].

Let M be a positive integer. There exist a sequence of real numbers $(h_n)_n$ for $n = 0, \dots, 2M - 1$, a function φ called the scaled function and a function ψ called the associated wavelet, such that

$$\begin{aligned}\varphi(x) &= \sqrt{2} \sum_{n=0}^{2M-1} h_n \varphi(2x - n), \quad \forall x \in \mathbb{R}, \\ \psi(x) &= \sqrt{2} \sum_{n=0}^{2M-1} g_n \varphi(2x - n), \quad \forall x \in \mathbb{R},\end{aligned}\quad (2)$$

where $g_n = (-1)^n h_{2M-1-n}$, $n = 0, \dots, 2M - 1$.

The functions φ and ψ have the following properties:

- φ and ψ are orthogonal, since
$$(\varphi, \psi) = \int_{\mathbb{R}} \varphi(x) \psi(x) dx = 0.$$
- The supports of φ and ψ lie in the closed interval $[0, 2M - 1]$.

Let

$$\begin{aligned}\varphi_{jk}(x) &= 2^{j/2} \varphi(2^j x - k); \quad V_j = \text{span}\{\varphi_{jk}, k \in \mathbb{Z}\}; \\ \psi_{jk}(x) &= 2^{j/2} \psi(2^j x - k); \quad W_j = \text{span}\{\psi_{jk}, k \in \mathbb{Z}\},\end{aligned}\quad (3)$$

the functions φ_{jk} and ψ_{jk} fulfill:

$$\int_{\mathbb{R}} \varphi_{jk}(x) \varphi_{i\ell}(x) dx = \delta_{k\ell}, \quad (4)$$

$$\int_{\mathbb{R}} \psi_{jk}(x) \psi_{i\ell}(x) dx = \delta_{k\ell} \delta_{ij}. \quad (5)$$

Relations (4) mean that $(\varphi_{jk})_k$ is an orthonormal basis of V_j for each j . Relations (5) mean that $(\psi_{jk})_k$ is an orthonormal basis of W_j for each j , and spaces W_j and W_i are orthonormal if $j \neq i$.

We therefore have

$$\begin{aligned}V_j &\subset V_{j+1}, \quad V_{j+1} = V_j \oplus W_j, \\ \bigcap_{j \in \mathbb{Z}} &= \{0\}, \quad L^2(\mathbb{R}) = \bigcup_{j \in \mathbb{Z}} V_j.\end{aligned}$$

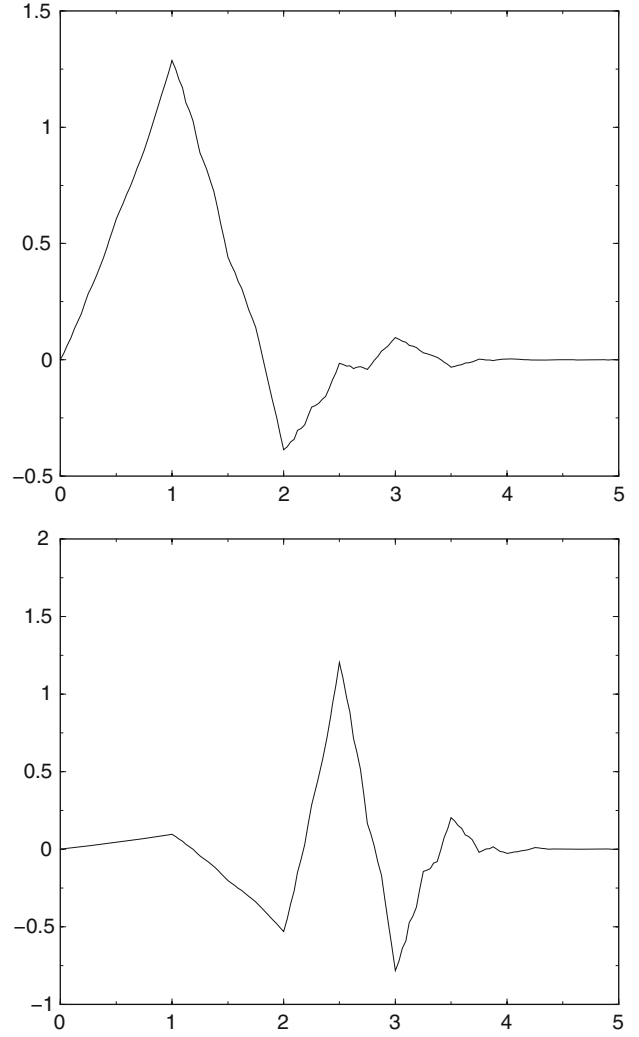


Fig. 2 The scale function and the associated Daubechies wavelet of order $M = 3$

The set of spaces $\{V_j, j \in \mathbb{Z}\}$ is called a multiresolution analysis of $L^2(\mathbb{R})$.

Figure 2 gives plots of the scale function and the associated Daubechies wavelet of order $M = 3$.

We can then obtain a multiresolution of $L^2_{\text{per}}(0, 1)$, the space of the periodic functions with a period equal to one, by periodizing the scaled function and the associated wavelet:

$$\begin{aligned}\phi_{jk}(x) &= 2^{j/2} \sum_{n \in \mathbb{Z}} \varphi(2^j(x+n) - k), \\ j &\geq 0, \quad k = 0, \dots, 2^j - 1;\end{aligned}\quad (6)$$

and likewise for the periodic associated wavelet.

We then perform a multiresolution of $L^2_{\text{per}}(\Omega)$, where $\Omega = (0, 1) \times (0, 1)$ with a tensor product. The periodic two-dimensional scale function becomes

$$\Phi_{jk}(x) = \phi_{jk_1}(x_1) \phi_{jk_2}(x_2), \quad \forall k = (k_1, k_2) \in \mathbb{Z}^2, \quad x \in \Omega, \quad (7)$$

and the three associated two-dimensional wavelets are:

$$\begin{aligned}\Psi_{jk}^1(x) &= \phi_{jk_1}(x_1)\psi_{jk_2}(x_2), \quad \forall k = (k_1, k_2) \in \mathbb{Z}^2, x \in \Omega, \\ \Psi_{jk}^2(x) &= \psi_{jk_1}(x_1)\phi_{jk_2}(x_2), \quad \forall k = (k_1, k_2) \in \mathbb{Z}^2, x \in \Omega, \\ \Psi_{jk}^3(x) &= \psi_{jk_1}(x_1)\psi_{jk_2}(x_2), \quad \forall k = (k_1, k_2) \in \mathbb{Z}^2, x \in \Omega.\end{aligned}\quad (8)$$

If we take Λ_j to denote the subset of \mathbb{Z}^2

$$\Lambda_j = \left\{ k \in \mathbb{Z}^2, 0 \leq k_1 \leq 2^j - 1, 0 \leq k_2 \leq 2^j - 1 \right\}, \quad (9)$$

and $\{\mathcal{V}_j, j \geq 0\}$ the multiresolution of $(L^2_{\text{per}}(\Omega))^2$, an element u in \mathcal{V}_j can be written

$$u(x) = \begin{pmatrix} u_1(x) \\ u_2(x) \end{pmatrix} \quad \text{with } u_d(x) = \sum_{k \in \Lambda_j} u_d^k \Phi_{jk}(x) \quad \forall x \in \Omega.$$

Comment 2

- The Daubechies wavelets are orthogonal for the scalar product of $(L^2_{\text{per}}(\Omega))^2$, and they are only implicitly given by the sequence $\{h_n\}_{n=0, \dots, 2M-1}$ (see 2).
- Unfortunately, the length of the support is very large. For example, if $M = 3$, the size of the support is in the $[0, 5]$ range. These values can be compared with those obtained using P2 finite elements, where the support is in the $[0, 2]$ interval. The number of non vanishing elements in the rigidity matrix will therefore be larger with the Daubechies wavelet method.
- These functions are not very regular and they are not symmetric (see Fig. 2). The consequences of these properties will be seen in Sect. 4.

3.2 B-spline wavelets

In order to avoid the problems due to the orthogonality of wavelets, bi-orthogonal wavelets have been introduced [6]. This procedure was based on a multiresolution analysis. It can be explained as follows:

- Define two sequences of embedded subspaces:

$$\begin{aligned}\dots &\subset V_{-2} \subset V_{-1} \subset V_0 \subset V_1 \subset V_2 \subset \dots \\ \dots &\subset \tilde{V}_{-2} \subset \tilde{V}_{-1} \subset \tilde{V}_0 \subset \tilde{V}_1 \subset \tilde{V}_2 \subset \dots\end{aligned}$$

- Define W_j (\tilde{W}_j resp.) the complementary space of V_j into V_{j+1} (\tilde{V}_j into \tilde{V}_{j+1} resp.), such that

$$V_j \perp \tilde{W}_j, \quad \tilde{V}_j \perp W_j.$$

- We therefore have two scale functions (φ and $\tilde{\varphi}$) and two wavelets (ψ and $\tilde{\psi}$) such that

$$\begin{aligned}\int_{\mathbb{R}} \varphi(x)\tilde{\varphi}(x-k)dx &= \delta_{0k}, \quad \forall k \in \mathbb{Z}, \\ \int_{\mathbb{R}} \psi(x)\tilde{\psi}(x-k)dx &= \delta_{0k}, \quad \forall k \in \mathbb{Z}, \\ \int_{\mathbb{R}} \varphi(x)\tilde{\psi}(x-k)dx &= 0, \quad \forall k \in \mathbb{Z}, \\ \int_{\mathbb{R}} \tilde{\varphi}(x)\psi(x-k)dx &= 0, \quad \forall k \in \mathbb{Z},\end{aligned}\quad (10)$$

- A function f is decomposed into

$$\begin{aligned}s_{j_0k} &= \int_{\mathbb{R}} f(x)\varphi_{j_0k}(x)dx, \quad \forall k \in \mathbb{Z}, \\ d_{jk} &= \int_{\mathbb{R}} f(x)\tilde{\psi}_{jk}(x)dx, \quad \forall j \geq j_0, k \in \mathbb{Z}\end{aligned}$$

and

$$f(x) = \sum_{k \in \mathbb{Z}} s_{j_0k} \tilde{\varphi}_{j_0k}(x) + \sum_{j \geq j_0} \sum_{k \in \mathbb{Z}} d_{jk} \psi_{jk}(x).$$

- Therefore, four filters are necessary:

$$\begin{aligned}\varphi(x) &= \sqrt{2} \sum_{n=0}^N h_n \varphi(2x-n); \\ \tilde{\varphi}(x) &= \sqrt{2} \sum_{n=0}^{\tilde{N}} \tilde{h}_n \tilde{\varphi}(2x-n); \\ \psi(x) &= \sqrt{2} \sum_{n=0}^N g_n \varphi(2x-n); \\ \tilde{\psi}(x) &= \sqrt{2} \sum_{n=0}^{\tilde{N}} \tilde{g}_n \tilde{\varphi}(2x-n).\end{aligned}\quad (11)$$

Comment 3

- The scale function φ is often a B-Spline [6,8]. In this case, we define the B-spline scale function of order N as N convolutions of the characteristic function on $[0, 1]$. The B-spline of order 2 is the P1 finite element on \mathbb{R} , and the B-spline of order 3 is plotted in Fig. 3. This function is differentiable, piecewise polynomial and of order two. The support of this function lies in the $[0, 3]$ range, and this function is symmetric.
- The choice of \tilde{N} , the size of the filter \tilde{h} , is much more difficult. The larger \tilde{N} is, the more regular $\tilde{\varphi}$ and $\tilde{\psi}$ will be. But the support of these functions will also increase. In order to give all four functions φ , $\tilde{\varphi}$, ψ and $\tilde{\psi}$ the

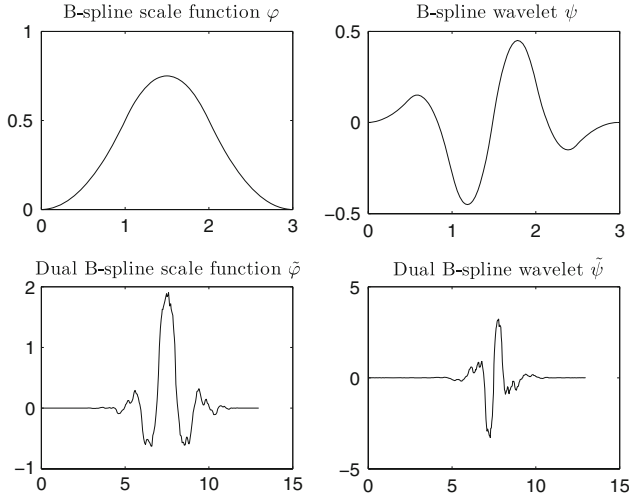


Fig. 3 The B-Spline wavelet of order $M = 3$

same regularity, one can take $\tilde{N} > 1.5N$. Examples of functions φ , $\tilde{\varphi}$, ψ and $\tilde{\psi}$ are given in [6].

3.3 Operator discretization

In this section, we will focus on solving problem P_Y . This problem is solved here using a wavelet-element method [36] with Daubechies wavelets [7] or B-Spline wavelets [6,8]. This method is based on the standard form of the discretized elastostatics operator [4]. Details of this method can be found in our previous papers [10, 12, 13].

In what follows, without any loss of generality, we will consider a two dimensional problem using the plane deformations hypothesis. The stress and the deformation tensors will therefore be taken to be vectors of \mathbb{R}^3 :

$$\sigma = \begin{pmatrix} \sigma_{11} \\ \sigma_{22} \\ \sigma_{12} \end{pmatrix}$$

and so on for the deformation tensor ε . We will also identify the elasticity operator with a 3×3 matrix denoted C on the representative volume and A on the homogeneous equivalent material, such that

$$\sigma = C\varepsilon.$$

More specifically, the solution u of P_Y is approximated by

$$u(y) = \sum_{k \in \mathbb{Z}^2} u_{jk} \Psi_{jk}(y) \quad y \in Y, \quad (12)$$

where $\Psi_{jk}(y) = 2^j \Psi(2^j y - k)$ is a localized function around the point $y = 2^{-j}k$. Since the function Ψ is compactly supported, the sum can be written in a finite dimensional subspace of \mathbb{Z}^2 , denoted Λ_j . Using test functions of this kind,

the projection of the linear elasticity tensor

$$a(u, v) = \int_Y C e(u) : e(v) dy$$

is a matrix \mathcal{K} defined by

$$[\mathcal{K}] = [\mathcal{K}_{i\ell}]_{i\ell \in \Lambda_j},$$

where $\mathcal{K}_{i\ell}$ is a 2×2 elementary matrix

$$\mathcal{K}_{i\ell} = \begin{bmatrix} F_{11}^{11} + F_{22}^{33} & F_{12}^{12} + F_{21}^{33} \\ F_{21}^{12} + F_{12}^{33} & F_{22}^{22} + F_{11}^{33} \end{bmatrix},$$

$$\text{with } F_{\eta\xi}^{\alpha\beta} = \int_Y C_{\alpha\beta}(x) \Psi_{j_i, \eta}(y) \Psi_{j_\ell, \xi}(y) dy.$$

Since the coefficients $C_{\alpha\beta}$ are piecewise constant, using the Haar wavelet

$$\theta(y) = \begin{cases} 1 & \text{if } y \in [0, 1], \\ 0 & \text{if not} \end{cases}$$

one can then write $C_{\alpha\beta}$ (we will omit α and β from now on):

$$C(y) = \sum_{n \in \mathbb{Z}^2} C_n \Theta_{jn}(y),$$

where $\Theta_{jn}(y) = 2^j \theta(2^j y_1 - n_1) \theta(2^j y_2 - n_2)$. Elements of the stiffness matrix are coefficients such as

$$\int_Y \Theta_{jn}(y) \Psi_{jk, \eta} \Psi_{j\ell, \xi}(y).$$

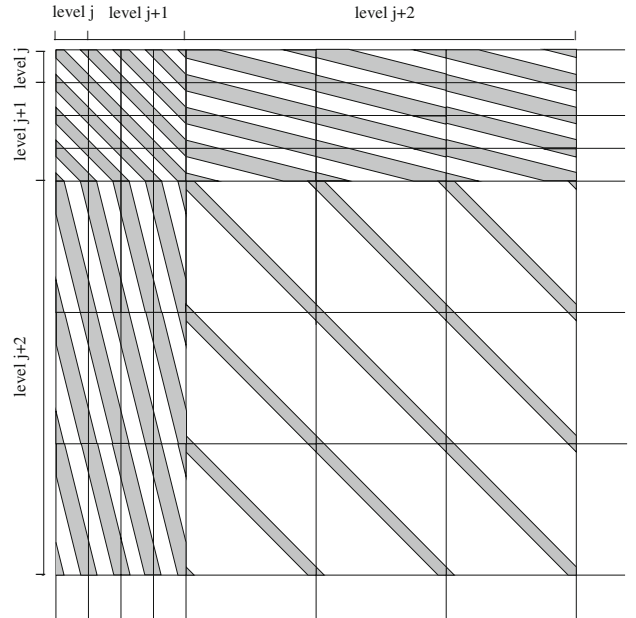


Fig. 4 Particular form of the stiffness matrix discretized with a wavelet method

Using the scale relation (2), these coefficients are computed once and for all without any approximation, after diagonalizing a small dimensional matrix [4,9,10].

Due to the particular type of wavelet basis involved (see formula 5), the discrete stiffness matrix takes the form plotted in Fig. 4. When it is necessary to solve a linear system with a matrix of this kind, a multigrid method gives excellent results.

Comment 4 *In what follows, the image of the microstructure will be composed of square pixels (as in Fig. 1), and this explains the use of Haar wavelets for the discretization of the elasticity coefficients $C_{\alpha\beta}$. One can also imagine that these coefficients could be given after performing digitization and filtering, using other types of wavelet based on a camera image. Note that the Jpeg2000 norm is based on the use of Daubechies wavelets [5,33].*

In this case, the approach developed here can be extended only by replacing the Haar basis by the wavelet used in the filtering step.

4 Numerical results

In this part of the paper, numerical tests on Al/SiC and resin/glass composites are presented. The effects of two parameters are studied: the volume fraction of each component (Aluminum and Silicium or Resin and Glass) and the distribution of each material in the microstructure. With each volume fraction, approximately 5000 draws are performed and results are studied statistically.

The elementary representative volume will be represented by an image with 32×32 pixels as proposed by Wriggers et al. [37]. The discretization of this domain will be carried out with 256×256 wavelet elements. The numerical results obtained in this study were not significantly different from those obtained using finer discretizations with 512×512 or 1024×1024 wavelet elements, for example.

The pixels corresponding to the second material are chosen randomly, using a uniform law.

The aim of this paragraph is to show that, even if after each draw s the homogeneous equivalent material with elasticity tensor equal to A_s is not isotropic, the mean elasticity tensor on the draws $\bar{A} = \langle A_s \rangle_s$ becomes isotropic and one can define “mean” bulk and shear moduli \bar{K} and $\bar{\mu}$ from \bar{A} .

In [37], a different approach was used. For each sample s , the authors computed the effective bulk and shear moduli:

$$3K_s^* = \frac{\langle tr\sigma_s/3 \rangle_\Omega}{\langle tr\varepsilon_s/3 \rangle_\Omega} \quad \text{and} \quad 2\mu_s^* = \sqrt{\frac{\langle \sigma'_s \rangle_\Omega : \langle \sigma'_s \rangle_\Omega}{\langle \varepsilon'_s \rangle_\Omega : \langle \varepsilon'_s \rangle_\Omega}},$$

where $\sigma' = \sigma - (tr\sigma/3)Id$ and $\varepsilon' = \varepsilon - (tr\varepsilon/3)Id$. They then studied the properties of the mean values of these quantities in the samples: $\bar{K}^* = \langle K_s^* \rangle_s$ and $\bar{\mu}^* = \langle \mu_s^* \rangle_s$.

4.1 AlSiC composite

First we focus on AlSiC composites having the following properties: the Young’s modulus is equal to $E = 0.41 \cdot 10^{+6}$ MPa and the Poisson’s ratio is equal to $\nu = 0.19$ in the case of silicium, and the Young’s modulus is equal to $E = 0.72 \cdot 10^{+5}$ MPa and the Poisson’s ratio is equal to $\nu = 0.32$ in that of aluminum. We consider a two-dimensional material, and we assume the plane stress hypothesis to be valid.

The changes in each elasticity coefficient are presented in Fig. 5 in the case of about 5000 microstructures at a volume fraction of 70%. The fluctuations can be seen to be very large.

On the other hand, if we look at the histogram of each component of the elasticity tensor, we can see that the values show a Gaussian distribution (Fig. 6).

The mean values on the n th first draws :

$$A_{ij}(n) = \frac{1}{n} \sum_{s=1}^n A_{ij}^s$$

versus the number of draws are given in Fig. 7, for each coefficient ij of the elasticity tensor. Coefficients $A_{ij}(n)$ in the case of all $i, j = 1, 2, 3$ can be seen here to converge on a mean value when the number n of draws increases.

If we study in detail the changes in the mean coefficients, we can see that the mean is obtained in quite a small number of draws (Fig. 8) and that the standard deviation is small in comparison with the coefficients. In the case presented in Fig. 8, i.e., at a volume fraction equal to 70%, the mean is equal to 12358 MPa and the standard deviation is equal to 768 MPa. The values are in the [12083,12682] range. In addition, after 2000 draws, the maximum standard deviation amounted to less than 0.01% of the coefficient. Therefore, 5000 draws suffice to obtain an accurate mean coefficient. The histogram in terms of polar coordinates (Fig. 9) shows the good distribution of the results in terms of the mean values. The values given in Fig. 7 show that the numerical limit is that of an **isotropic material**. In particular, we have $A_{13} = A_{23} = 0$ and $A_{11} = A_{22}$. It is therefore possible to compute the bulk and shear moduli of the limit material (Mean bulk and shear moduli).

In what follows, we take L-HS and U-HS to denote the Lower and Upper Hashin and Shtrikman bounds [16]. We take WAV to denote the Mean Value obtained using the Wavelet-element method. Figure 10 shows three phases: in the first phase, at volume fractions lower than 0.25, the L-HS and WAV values are very similar. The second phase corresponds to volume fractions of 0.25 to 0.95. In this phase, the WAV value is mid-way between the two HS bounds. In the third phase, at volume fractions above 0.95, the WAV values are similar to the values of U-HS bounds.

Fig. 5 Homogenized plane elasticity tensor versus draws (volume fraction 70%). Each peak gives the result of one test

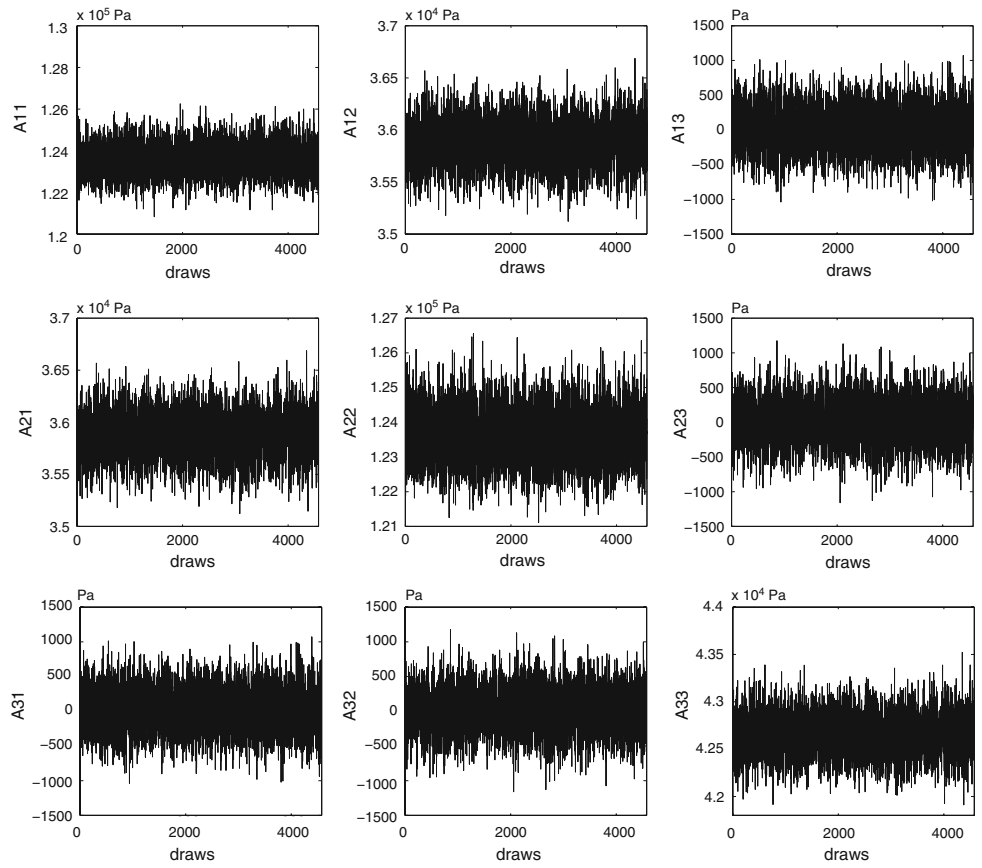


Fig. 6 Histogram of plane elasticity tensors (volume fraction 70%)

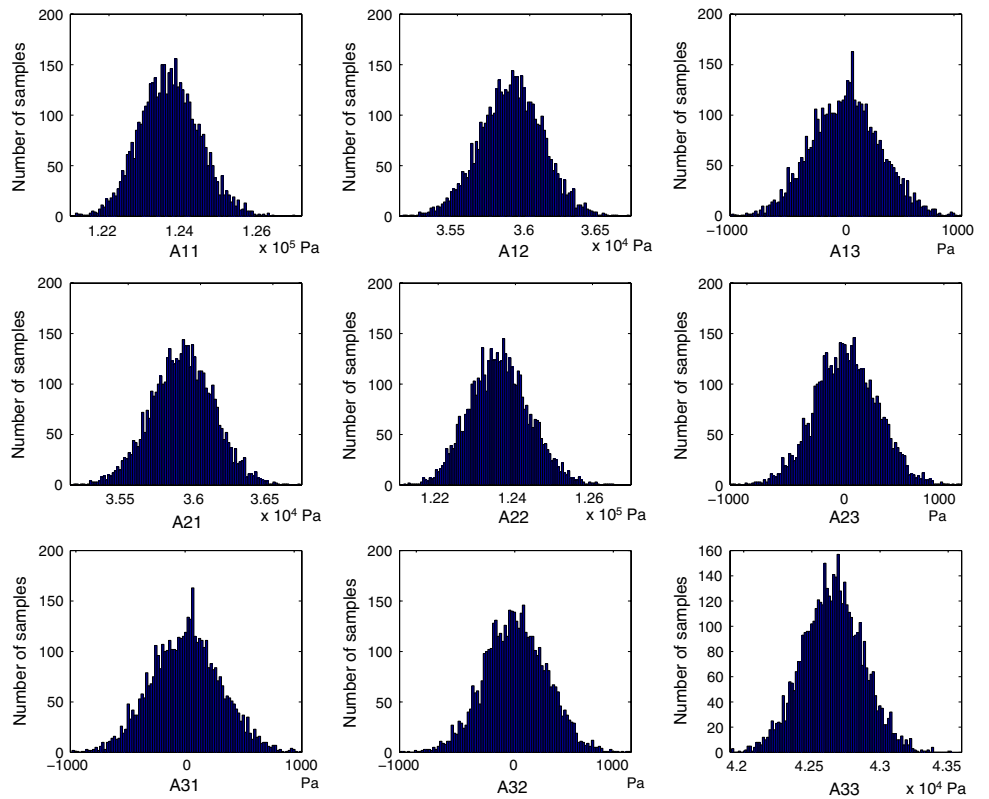


Fig. 7 Mean value based on the n th first draws of the homogenized elasticity tensor versus the number n of draws (volume fraction 70%)

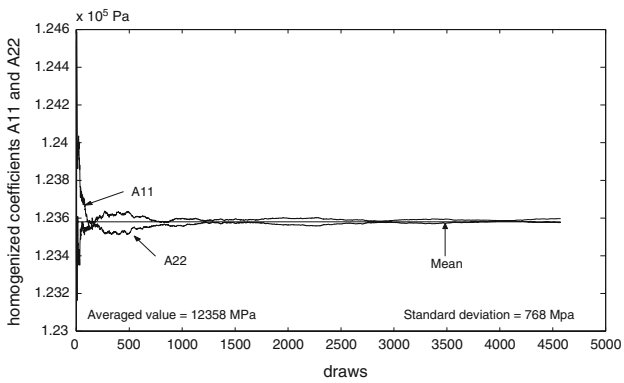
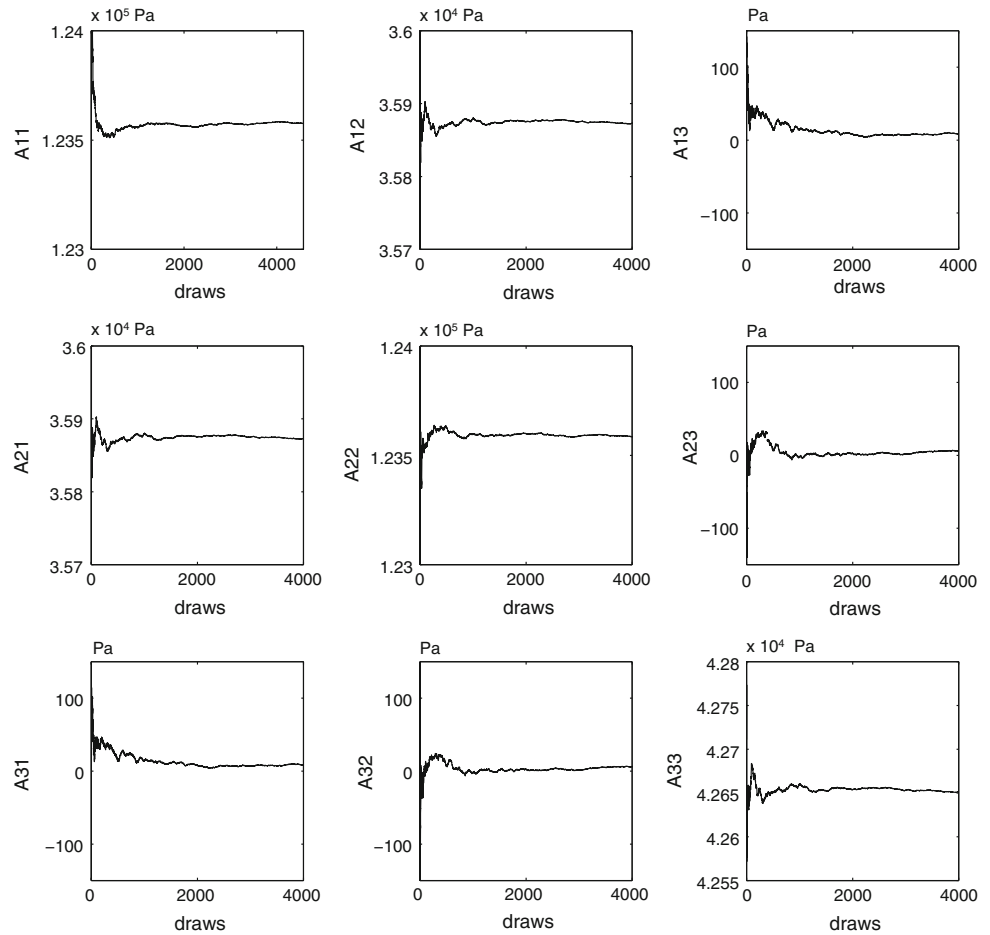


Fig. 8 Mean value based on the n th first draws of the homogenized elasticity coefficients A^{11} and A^{22} versus the number of draws (volume fraction 70%), compared with the mean value based on 7000 draws

If we compare the results obtained with the self-consistent schema on the shear modulus and at volume fractions lower than 0.5, we can see from Fig. 11 that at the lower volume fraction values (lower than 0.1), the L-HS value, the results based on the self-consistent schema (denoted SCS) and the WAV value are fairly similar. At higher volume fraction values ranging from 0.1 to 0.25, the L-HS and WAV values are

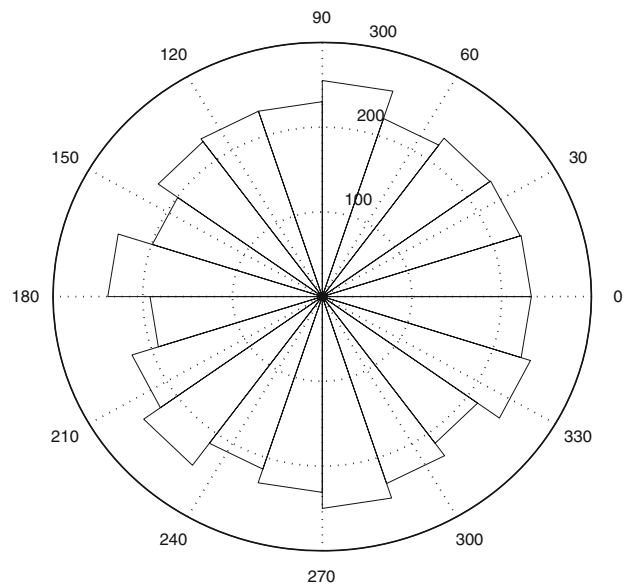


Fig. 9 Histogram in polar coordinates (volume fraction 70%, AISiC)

practically identical and the SCS value is lower than the other two. At volume fractions above 0.25 and below 0.4, the L-HS and SCS values are similar, and lower than the WAV value.

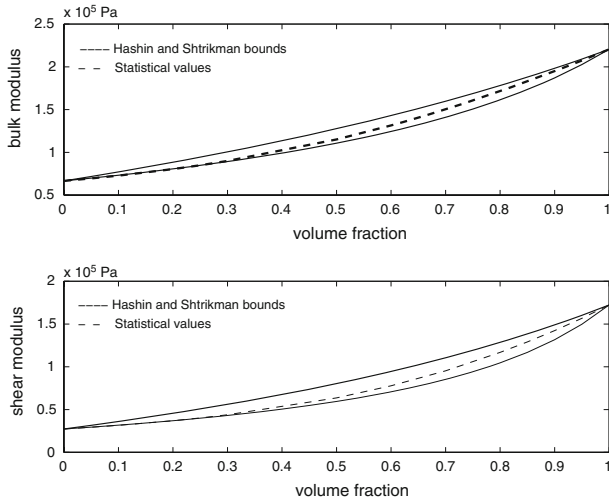


Fig. 10 Bulk and shear moduli and Hashin–Shtrikman bounds (AISiC)

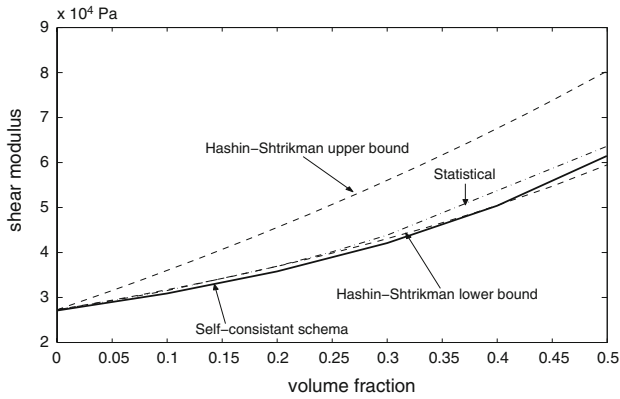


Fig. 11 Shear modulus, Hashin–Shtrikman bounds and self-consistent schema (AISiC)

4.2 Resin–glass composite

In the resin–glass composites studied here, the Young’s modulus is equal to $E = 0.73 \cdot 10^{+5}$ MPa and the Poisson’s ratio is equal to $\nu = 0.25$ in the case of the glass, and the Young’s modulus is equal to $E = 0.30 \cdot 10^{+4}$ MPa and the Poisson’s ratio is equal to $\nu = 0.40$ in that of the resin. We assume the existence of a two-dimensional material, and the plane stress hypothesis is assumed to be valid.

In this case, the difference between the properties of the two composites is greater than previously. The histograms plotted in polar coordinates in Figs. 11 and 12 show the good distribution of the mean results obtained at various glass and resin volume fractions (20% in Fig. 12 and 80% in Fig. 13).

Figure 14 shows that the behavior of this composite was similar to that observed in the case of the AISiC composite: the relative behavior can again be split into three phases. In the first part, at a volumic fraction below 0.35, the L-HS and WAV values were similar.

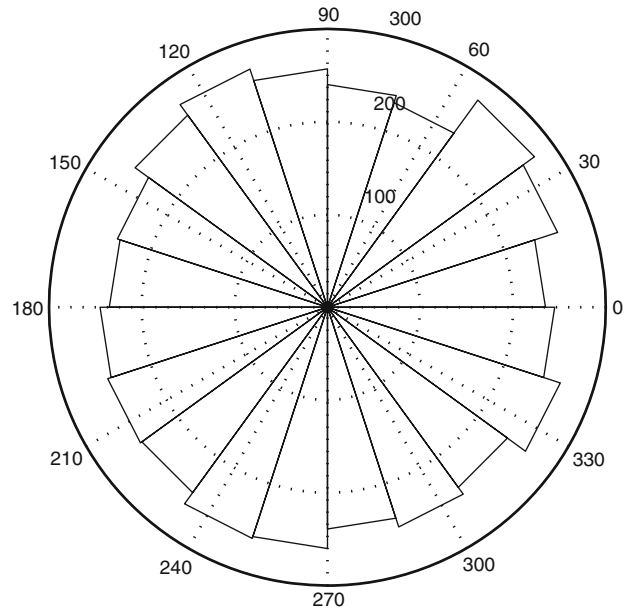


Fig. 12 Histogram in polar coordinate system (volume fraction 20%, resin/glass composite)

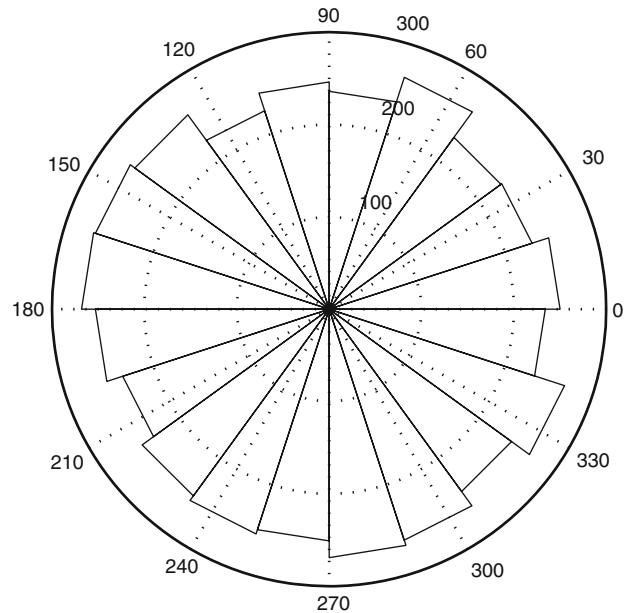


Fig. 13 Histogram in polar coordinate system (volume fraction 80%, resin/glass composite)

The second phase corresponds to volume fractions ranging between 0.35 and 0.99. In this phase, the WAV value is mid-way between the two HS bounds. In the third phase, the WAV value tangents the U-HS bounds.

4.3 Comparison between Daubechies wavelets and B-Spline wavelets

We end this section with a discussion about the wavelets.

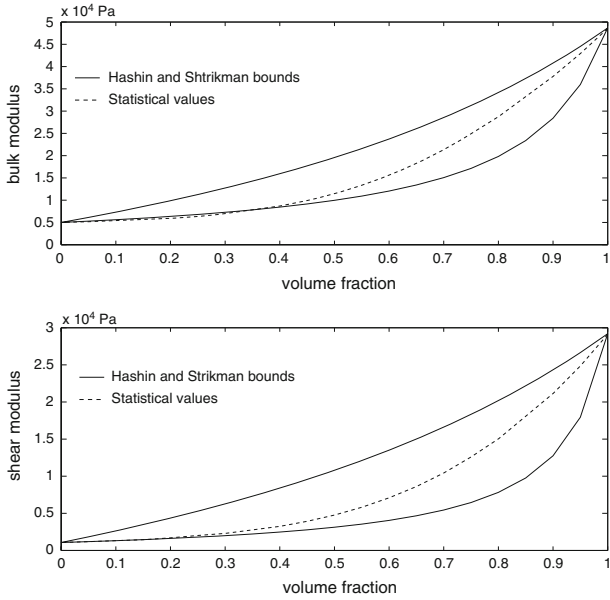


Fig. 14 Bulk and shear moduli and Hashin–Shtrikman bounds (resin/glass composite)

Table 1 Comparison between the bulk and shear moduli ($\times 10^3$ Pa) obtained using Daubechies and B-Splines wavelets, in Al/SiC (low contrast) and B-Splines (large contrast), with a volume fraction of the first component equal to 20%

		Bulk mod.	Shear mod.
Al/SiC	Daubechies	80.6	36.7
	B-Splines	83.0	36.9
Resin/glass	Daubechies	5.83	1.74
	B-Splines	6.25	1.70
Differences	Al/SiC	3%	0.5%
	Resin/glass	7%	2%

Results are averages based on 100 draws

Table 1 gives the bulk and shear moduli obtained with Al/SiC and resin/glass composites, using Daubechies and B-Splines wavelets. The volume fraction of the first component of the composite was equal to 20%, and the moduli were obtained by averaging on 100 draws.

In the case of the AlSiC composite (low contrast), the results given by the two discretization procedures (Daubechies and B-spline wavelets) were very similar (difference amounted to less than 3%); whereas with the resin/glass composite (large contrast), since the differences between the properties of the two materials were larger, the two discretization procedures did not give similar results. The differences increased by 7% in the bulk modulus and by 2% in the shear modulus. Moreover, the bulk modulus given by the Daubechies wavelets was outside the bounds, due to the lack of symmetry and regularity of Daubechies wavelets. Using the symmetric and C^1 B-spline wavelets, better results

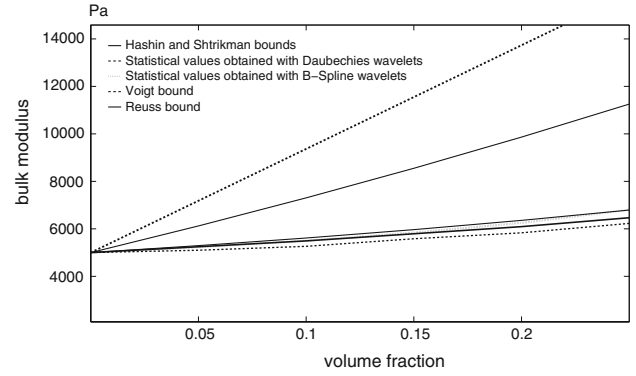


Fig. 15 Bulk moduli and Hashin–Shtrikman bounds obtained with Daubechies and B-spline wavelets (resin/glass composite)

were obtained and the average bulk modulus computed was very near the lowest Hashin and Shtrikman bound (see Figs. 14, 15).

We recall that the moduli have to be within the Hashin and Shtrikman bounds only in the asymptotic case of an infinite (sample length)/(particle length) ratio and purely isotropic macroscopic responses [16]. This was not the case here where the ratio was equal to 32.

In addition, the results obtained with the B-spline wavelets were always within the Voigt and Reuss bounds, contrary to the results obtained with the Daubechies wavelets. This shows that the use of B-spline wavelets improves the numerical procedure.

Comment 5 *Unlike the finite element method, the wavelet element method can be used with a single tool for the image processing, the image compression and the determination of the effective properties. In particular, this method does not require the use of Voronoi techniques. However, the solution of the linear systems can be compute less expensively using the finite element method [10].*

5 Concluding comments and perspectives

It is generally impossible to exactly determine the effective properties of random heterogeneous media. The most rigorous statements in the literature about these effective properties focus on the bounds. In this study, bounds of another kind were obtained in the form of an average and a standard deviation. One of the main results obtained here is the numerical convergence between the stochastic homogenization process with a mean solution, i.e., when the number of draws tends to infinity, the limit of the potential energy corresponding to a 'random lattice' is the potential energy of an isotropic material. The effective properties of this material depend on the volume fraction of each component. At lower volume fractions, the material has similar properties to those given by the

lower Hashin and Shtrickman bounds and the self-consistent schema. A numerical theorem is obtained. This result is consistent with those obtained in [22] using the finite element method and with an initial result obtained at low contrast in [25]. Note that this theorem is a generalization of rigorous mathematical stochastic homogenization results obtained in another context (scalar problems) [1, 2].

The method developed here, based on a wavelet transform procedure is highly efficient and makes it possible to avoid meshing the microstructure after each draw. In addition, since the wavelet transform method was developed for image processing purposes, it can be used to determine the microstructure with a good resolution and a reasonable number of degrees of freedom.

This study could be extended in two ways: first, by determining the effects of the shape of the lattices. We propose to study the same problem investigated here with different morphologies: n -pixels in one direction, sets of n -pixels in the neighborhood of a point, etc. Another possible approach would consist in studying the effective properties in the case of more complex behavior such that involved in piezoelectric coupling, thermomechanical coupling and non linear behavior [26, 29, 32]. This method lends itself to dealing with problems of this kind because it has proved to be a particularly efficient tool.

Acknowledgments The authors gratefully acknowledge R. Peyroux for helpful discussions, enlightening comments and self-consistent schema software.

References

1. Andrews KT, Wright S (1998) Stochastic homogenization of elliptic boundary-value problem with L^p -data. *Asymptotic Anal* 17:165–184
2. Beliaev AY, Kozlov SM (1996) Darcy equation for random porous media. *Commun Pure Appl Math* 49:1–34
3. Bensoussan A, Lions JL, Papanicolaou G (1978) Asymptotic analysis for periodic structures, 1st edn. North-Holland, Amsterdam
4. Beylkin G (1992) On the representation of operators in bases of compactly supported wavelets. *SIAM J Numer Anal* 29:1716–1740
5. Christopoulos CA, Ebrahimi T, Skodras AN (2000) Jpeg2000: the new still picture compression standard. In: *MULTIMEDIA '00: Proceedings of the 2000 ACM workshops on Multimedia*, ACM, New York, NY, USA, pp 45–49. doi:http://doi.acm.org/10.1145/357744.357757
6. Cohen A, Daubechies I, Feauveau JC (1992) Biorthogonal bases of compactly supported wavelets. *Commun Pure Appl Math* 45:465–560
7. Daubechies I (1992) Orthonormal bases of compactly supported wavelets. *Commun Pure Appl Math* 41:909–998
8. Deslaurier G, Dubuc S, Lemire D (1999) Une famille d'ondelettes bi-orthogonales sur l'intervalle obtenue par un schéma d'interpolation itérative. *Ann Sci Math du Québec* 23:37–48
9. Dumont S, Lebon F (1996a) Representation of plane elastostatics operators in Daubechies wavelets. *Comput Struct* 60:561–569
10. Dumont S, Lebon F (1996b) Wavelet-Galerkin method for periodic heterogeneous media. *Comput Struct* 61:55–65
11. Dumont S, Lebon F (1999) Wavelet-Galerkin method for plane elasticity. *Comput Appl Math* 8:127–142
12. Dumont S, Lebon F, Ould-Khaoua A (2000) A numerical tool for periodic heterogeneous media. Application to interface in Al/SiC composites. *ASME J Appl Mech* 67:214–217
13. Dumont S, Lebon F, Nguyen TTV (2001) Wavelets and PDE's: on two applications in solids mechanics. *Rev Cinc Math* 19:20–30
14. Dumont S, Goubet O, Ha-Duong T, Villon P (2006) Meshfree methods and boundary conditions. *Int J Numer Methods Eng* 67:989–1011
15. Garboczi E, Day A (1995) An algorithm for computing the effective linear elastic properties of heterogeneous materials; three-dimensional results for composites with equal phase Poisson ratio. *J Mech Phys Solids* 43:1349–1362
16. Hashin Z, Shtrickman S (1963) A variational approach to the theory of the elastic behaviour of multiphase materials. *J Mech Phys Solids* 11:127–140
17. Hazanov S, Huet C (1994) Order relationships for boundary condition effect in heterogeneous bodies smaller than representative volume. *J Mech Phys Solids* 42:1995–2011
18. Hill R (1963) Elastic properties of reinforced solid: some theoretical principles. *J Mech Phys Solids* 11:357–372
19. Hill R (1965) A self-consistent mechanics of composite materials. *J Mech Phys Solids* 13:213–222
20. Huet C (1990) Application of variational concepts to size effects in elastic heterogeneous bodies. *J Mech Phys Solids* 38:813–841
21. Huet C, Wriggers P, Zohdi T (2001) A method of substructuring large-scale computational micromechanical problems. *Comput Methods Appl Mech Eng* 190:5639–5656
22. Kanit T, Forest S, Galliet I, Mounoury V, Jeulin D (2003) Determination of the size of the representative volume element for random composite: statistical and numerical approach. *Int J Solids Struct* 40:3647–3679
23. Kanit T, N'Guyen F, Forest S, Jeulin D, Reed M, Singleton S (2006) Apparent and effective physical properties of heterogeneous materials: representativity of samples of two materials from food industry. *Comput Methods Appl Mech Eng* 195:3960–3982
24. Lebon F (2000) Small parameter, homogenization and wavelets. *Rev Cinc Math* 18:191–200
25. Lebon F, Dumont S (2004) Novel approaches in civil engineering. *Lecture Notes in Applied Computational Mechanics*, vol 14. Springer, chap Application to the wavelet-element method to linear random materials, Berlin, pp 329–337
26. Lebon F, Rodriguez R, Lopez-Realpozo JC, Bravo-Castillero J, Guinovart-Diaz R, Mesejo A (2006) Effective properties of nonlinear laminated composites with perfect adhesion. *ASME J Appl Mech* 73:174–178
27. Michel JC, Moulinec H, Suquet P (2001) A computational method for linear and nonlinear composites with arbitrary phase contrast. *Int J Numer Methods Eng* 52:139–160
28. Peyroux R (1990) Caractéristiques thermoélastiques de matériaux composites à fibres courtes. Ph.D. thesis, Montpellier 2 University
29. Reikik A, Bornert M, Auslender F, Zaoui A (2005) A methodology for an accurate evaluation of the linearization procedures in nonlinear mean field homogenization. *C R Mécanique* 333:789–795
30. Sab K (1992) On the homogenization and the simulation of random materials. *Eur J Mech A Solids* 11:585–607
31. Sanchez-Palencia E, Zaoui A (1987) Homogenization techniques for composite media. *Lecture notes in physics*. Springer, Berlin
32. Suquet P (1995) Overall properties of nonlinear composites: a modified secant moduli theory and its link with Ponte Castaneda's nonlinear variational procedure. *C R Mécanique* 320:563–571

33. Taubman D, Marcellin M (2002) JPEG2000 Image compression fundamentals. Standards and practices, series: the international series in engineering and computers science. Kluwer, US
34. Torquato S (1991) Random heterogeneous media: microstructure and improved bounds on effective properties. *Appl Mech Rev* 44:37–76
35. Torquato S (2002) Random heterogeneous materials. Springer, Berlin
36. Wells RO, Zhou X (1995) Wavelet solutions for the Dirichlet problem. *Numerische Mathematik* 70:379–396
37. Wriggers P, Zohdi T (2001) Aspects of the computational testing of the mechanical properties of microheterogeneous material samples. *Int J Numer Methods Eng* 50:2573–2599
38. Wriggers P, Zohdi T (2005) Introduction to computational micro-mechanics. Springer, Berlin